Adaptive Path Following for Unmanned Aerial Vehicles in Time-Varying Unknown Wind Environments*

Bingyu Zhou[1], Harish Satyavada[2] and Simone Baldi[1]

***Abstract*— In this paper, an adaptive control scheme for Unmanned Aerial Vehicles (UAVs) path following under slowly time-varying wind is developed. The proposed control strategy integrates the path following law based on the vector field method with an adaptive term counteracting the effect of wind's unknown component. The control strategy is developed and numerically simulated for straight line and orbit following scenarios. In particular, it is shown that the path following error is bounded under slowly time-varying unknown wind and converges to zero for unknown constant wind. Numerical simulations illustrate that, in environments with unknown and slowly time-varying wind conditions, the proposed method compensates for the lack of knowledge of the wind vector, and attains a smaller path following error than state-of-the-art vector field method.**

I. INTRODUCTION

Unmanned aerial vehicles (UAVs) are versatile in many applications nowadays including military, agriculture, geographical exploration and so on. Most tasks in these application fields, like the military surveillance at a certain target, the rescue task in the forest fire, rely on the accurate and robust path generator and path tracking controller in UAVs. A path tracking controller in place of the human pilot plays a key role in manipulating UAVs under hazard environment. The challenge of the path following controller design stems from the wind disturbance, UAV dynamic characteristics and the quality of the sensors. In this paper, the influence of wind on UAV behavior is the main consideration in the path following design procedure.

In [1] the authors point out the difference between tracking a reference time signal and following a geometric path. Generally, the latter is less restrictive than the former since there is one extra degree of freedom to select the time law for the path variable. This paper is focused on the following of geometric paths.

Several methods for UAV path following have been already proposed and tested on actual UAV platforms. In [2], state-of-the-art path following algorithms in 2D are summarized and compared with each other using two metrics: total control effort and total cross-track error. Five algorithms are evaluated in [2] namely carrot-chasing algorithm, nonlinear guidance law (NLGL) [3], vector-field (VF)-based path following, LQR-based path following [4] [5] and pure pursuit with line-of-sight (PLOS)-based path following [6]. Monte Carlo simulations show that the VF path following technique is more accurate than the other methods. Furthermore, the simulations point out that a good wind estimator is beneficial to the performance of any path following algorithm.

The vector field path following algorithm is widely used in robotics, marine vehicles and autonomous automobiles. Its basic concept is to construct the vector field around the desired path to provide the course commands to the vehicle. Usually the path following laws are derived from Lyapunov stability analysis which guarantees the globally stable convergence to the desired path. The implementation of this concept is shown in [7] and [8]. Another variation of Lyapunov vector field is proposed in [9], which is called tangent vector field guidance. This new vector field method outperforms the classic Lyapunov vector field in most cases, but it is not valid when the current position of the UAV is inside the desired orbit path.

However, VF methods work under the assumptions of a perfectly known constant wind disturbance. In this paper, a novel vector field path following strategy extends the standard VF approach in [7]. The work in [7] proposes a vector field path following controller to generate desired course inputs for straight line and orbit path respectively. Lyapunov stability arguments are used to prove the asymptotic decay of path following errors. The main contribution of this paper is to extend the standard vector field path following strategy to uncertain and possibly time-varying wind scenarios. The motivation of this work stems from uncertain real-life conditions in which unknown and possibly time-varying wind components might add up to a constant wind component. An accurate UAV path following algorithm must then be able to handle this scenario. In this work, the path following control law is augmented with an estimator counteracting the effects of the unknown wind component, thus resulting in an adaptive vector field path following strategy. Stability analysis is performed via Lyapunov methods. In particular, it is shown that the path following error is bounded under slowly time-varying unknown wind and converges to zero for unknown constant wind. Performance improvement over a standard VF method is demonstrated in numerical simulations.

The rest of the paper is organized as follows. In section II, the UAV path following problem and the kinematics of UAV movement are described. The path following algorithms for straight line and orbit are introduced in section III, together with simulation results. The comparison between the standard vector field method and the proposed adaptive

*This work has been partially sponsored by autoNomous, self-Learning, OPTImal and compLete Underwater Systems (NOPTILUS), Project Number: 270180, Funded by: EU FP7-ICT-2009.6. http://www.noptilus-fp7.eu/.

[1]Bingyu Zhou and Simone Baldi are with Delft Center for Systems and Control, 3ME, Delft University of Technology, 2628 CD, Delft, The Netherlands bryan-by@hotmail.com;S.Baldi@tudelft.nl

[2]Harish Satyavada is with GE Global Research (Wind Lab), Whitefield, Bangalore, India satyavada93@gmail.com

vector field method is discussed in section IV. Finally, section V concludes this work.

II. Problem Description

The vector field (VF) method is based on specifying a desired course at a certain coordinate. This method is applicable for straight line and orbit arcs. More complicated paths can be segmented with straight lines and arcs ([9], [10]).

Some assumptions are listed here to clarify the limitations and study ground of this paper.

Assumption 1: Altitude and airspeed (V_a) are held constant by the longitudinal control of UAV.

Assumption 2: The UAV is equipped with the course-hold loop devices whose dynamics can be modeled as the first-order system

$$\dot{\chi}' = \alpha(\chi_c - \chi')$$

where χ' is the real course of the UAV, i.e. the angle between its ground velocity and the horizontal axis in the earth frame, χ_c is the command course from the controller, and α is a known positive constant that defines the response speed of the course-hold loop.

Assumption 3: The UAV course is measurable.

Assumption 4: The wind field consists of a constant component with magnitude W, angle ψ_w and a slowly time-varying unknown component with amplitude $A(t)$ and angle $\psi_A(t)$.

Remark 1: Assumptions 1, 2 and 3 are standard in most VF strategies ([7], [8], [9], [11], [12]). Assumption 4 relaxes the classical assumption where the wind vector is completely known.

In the numerical studies done in this work, we take the following environmental conditions: the magnitude of the time-varying component is changing over time in a co-sinusoidal fashion with frequency 0.1 rad/sec, the angle of the time-varying component is changing in a sinusoidal fashion with frequency 0.1 rad/sec. All the parameters related to the time-varying component of the wind are unknown to the designer. The designer only knows the constant component of the wind, whose parameters are considered as:
Constant wind's amplitude: $W = 6$;
Constant wind's angle: $\psi_w = 230°$;
Time-varying wind's amplitude: $A(t) = 3\cos(0.1t)$;
Time-varying wind's angle: $\psi_A(t) = \pi\sin(0.1t)$.

Under assumptions 1-4, the relationship between UAV airspeed, ground velocity and wind velocity can be illustrated in Fig. 1, resulting in the following navigational dynamics of the UAV:

$$\begin{aligned}\dot{x} &= V_a\cos\psi + W\cos\psi_w + A\cos\psi_A \\ \dot{y} &= V_a\sin\psi + W\sin\psi_w + A\sin\psi_A\end{aligned} \tag{1}$$

where ψ is the heading angle between airspeed and horizontal axis in earth frame, V_a is UAV airspeed, W and A are the amplitude of constant and time-varying part of wind, ψ_w and ψ_A are the angle between constant or time-varying part of wind velocity and x axis in the earth frame. x and y are the coordinate of the earth frame. The value of W and ψ_w can be obtained from historical data of wind velocity, while $A(t)$ and $\psi_A(t)$ can be regarded as disturbances which are slowly changing over time.

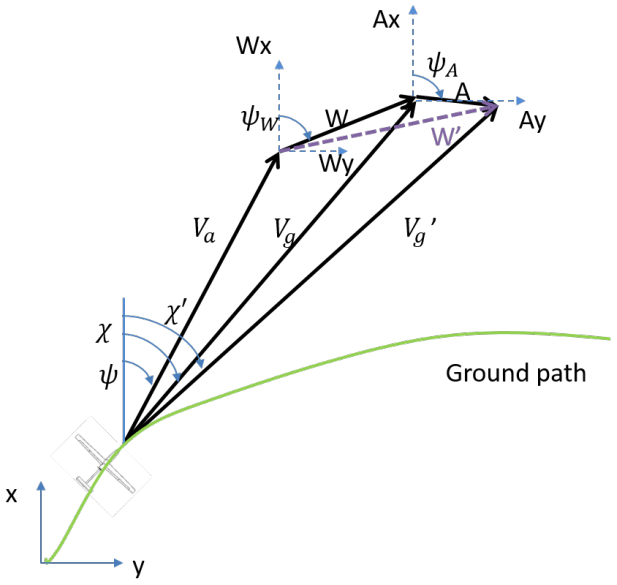

Fig. 1. UAV kinematics and relations between airspeed, ground velocity and wind velocity

From Fig. 1, the UAV velocity in x, y direction can also be expressed by the ground speed and course

$$\begin{aligned}\dot{x} &= V_g'\cos\chi' \\ \dot{y} &= V_g'\sin\chi'\end{aligned} \tag{2}$$

where V_g' is the ground velocity of UAV. Note that V_g' is not measurable since the time-varying wind influences the amplitude of ground velocity.

The overall wind field is denoted with amplitude W' and angle $\psi_{w'}$, which are a combination of constant and time-varying parts

$$\begin{aligned}W'\cos\psi_{w'} &= W\cos\psi_w + A\cos\psi_A \\ W'\sin\psi_{w'} &= W\sin\psi_w + A\sin\psi_A\end{aligned} \tag{3}$$

In the design of vector fields and wind estimators, two fundamental paths are considered: the straight line and orbit paths. In the numerical section, these two elementary paths are combined to demonstrate the ability of path following for more complicated trajectories.

III. Path Following Algorithm

A. Straight Line Following

The objective of straight line following is to steer the UAV to the desired line and adjust its course to keep along with the line. In another words, the vector field should guide the UAV to follow the desired straight line. With respect to [7], a small modification is presented in order to generalize the method for arbitrary lines and arbitrary directions. The error

distance e from UAV to desired line in y direction and the desired course χ_d are defined as:

$$e = y - (ax + b)$$
$$\chi_d = i\chi^\infty \frac{2}{\pi}\tan^{-1}(ke) + \tan^{-1}(a)$$

where $ax+b$ defines the line equation of desired path, (x, y) is the coordinate of UAV in the ground reference frame, i defines the direction of UAV movement. When $i = 1$, the UAV goes to the negative direction of x axis. When $i = -1$, the UAV goes to the positive direction of x axis. k is a positive constant which influences the rate of course transition from χ^∞ to steady state course $\tan^{-1}(a)$.

Similar to the Lyapunov stability analysis in [7], Lyapunov function $\mathcal{V}_1 = \frac{1}{2}e^2$ can be used to argue that e will converge to zero if $\chi' \to \chi_d$.

$$\begin{aligned}\dot{\mathcal{V}}_1 &= e(\dot{y} - a\dot{x}) \\ &= eV_g'(\sin\chi_d - a\cos\chi_d) \\ &= eV_g'\frac{\sin(i\chi^\infty\frac{2}{\pi}\tan^{-1}(ke))}{\cos(\tan^{-1}a)}\end{aligned}$$

If $e < 0, i < 0$ and χ^∞ is restricted in the range $(0, \frac{\pi}{2}]$, then $0 < i\chi^\infty\frac{2}{\pi}\tan^{-1}(ke) < \frac{\pi}{2}$ and $-\frac{\pi}{2} < \tan^{-1}(ke) < \frac{\pi}{2}$. If $e < 0, i > 0$ and χ^∞ is restricted in the range $(0, \frac{\pi}{2}]$, then $-\frac{\pi}{2} < i\chi^\infty\frac{2}{\pi}\tan^{-1}(ke) < 0$ and $\frac{\pi}{2} < \tan^{-1}(ke) < \frac{3\pi}{2}$. If $e > 0, i < 0$ and χ^∞ is restricted in the range $(0, \frac{\pi}{2}]$, then $-\frac{\pi}{2} < i\chi^\infty\frac{2}{\pi}\tan^{-1}(ke) < 0$ and $-\frac{\pi}{2} < \tan^{-1}(ke) < \frac{\pi}{2}$. If $e > 0, i > 0$ and χ^∞ is restricted in the range $(0, \frac{\pi}{2}]$, then $0 < i\chi^\infty\frac{2}{\pi}\tan^{-1}(ke) < \frac{\pi}{2}$ and $\frac{\pi}{2} < \tan^{-1}(ke) < \frac{3\pi}{2}$. For all of the cases above, $\dot{V}_1$ is smaller than zero for $e \neq 0$, which means that error distance e converges to zero asymptotically if $\chi' \to \chi_d$.

Let $\mathcal{V}_2 = \frac{1}{2}\tilde{\chi}'^2$, where $\tilde{\chi}' = \chi' - \chi_d$ is the error between UAV course and desired course. The derivative of $\mathcal{V}_2$ is

$$\begin{aligned}\dot{\mathcal{V}}_2 &= \tilde{\chi}'\dot{\tilde{\chi}}' \\ &= \tilde{\chi}'(\alpha(\chi_c - \chi') - i\chi^\infty\frac{2}{\pi}\frac{k\dot{e}}{1+(ke)^2}) \\ &= \tilde{\chi}'(\alpha(\chi_c - \chi') - i\chi^\infty\frac{2}{\pi}\frac{k}{1+(ke)^2}V_g'(\sin\chi' - a\cos\chi'))\end{aligned}$$

Ideally, if we choose the command course as:

$$\chi_c = \chi' + \frac{i}{\alpha}\chi^\infty\frac{2}{\pi}\frac{k}{1+(ke)^2}V_g'(\sin\chi' - a\cos\chi') - \frac{\kappa}{\alpha}sat(\frac{\tilde{\chi}'}{\epsilon}) \tag{4}$$

where sat is the saturation function used to eliminate chattering of sign function.

$$sat(x) = \begin{cases} x, & \text{if} \quad |x| < 1 \\ sign(x) & \text{otherwise}\end{cases}$$

and $\kappa > 0, \epsilon > 0$ are the parameters that control the shape of the trajectories on sliding surface and the width of the transition region around the sliding surface respectively. Then the derivative of $\mathcal{V}_2$ equals

$$\dot{\mathcal{V}}_2 = \begin{cases} -\frac{\kappa}{\epsilon}\tilde{\chi}'^2 & \text{if} \quad |\frac{\tilde{\chi}'}{\epsilon}| < 1 \\ -\kappa|\tilde{\chi}'| & \text{otherwise}\end{cases}$$

which is always negative semi-definite. We conclude that χ' converges to the desired course χ_d in finite time.

However, the control law in (4) cannot be implemented in practice since V_g' is not measurable. In this case, an estimator is designed to estimate the ground velocity of UAV. The control law will be modified as:

$$\chi_c = \chi' + \frac{i}{\alpha}\chi^\infty\frac{2}{\pi}\frac{k}{1+(ke)^2}\hat{V_g}'(\sin\chi' - a\cos\chi') - \frac{\kappa}{\alpha}sat(\frac{\tilde{\chi}'}{\epsilon}) \tag{5}$$

where $\hat{V_g}'$ is the estimated value of V_g'. The following stability result can be stated.

Theorem III.1: In straight line following scenario, the command course (5) and the estimator

$$\dot{\hat{V}}_g' = -\Gamma\rho\tilde{\chi}' i\chi^\infty\frac{2}{\pi}\frac{k}{1+(ke)^2}(\sin\chi' - a\cos\chi') - \sigma\Gamma\hat{V_g}' \tag{6}$$

with $\Gamma > 0$ being the estimation gain and $\sigma > 0$ being a switching σ-modification parameter, guarantees that the tracking error converges to zero for unknown constant winds and stays bounded for unknown slowly time-varying wind.

Proof: The adaptive law of $\hat{V_g}'$ is derived based on the Lyapunov argument below. Let $\Theta = \hat{V_g}' - V_g'$ be the estimation error. Consider the Lyapunov function $\mathcal{V}_e = \mathcal{V}_1 + \rho\mathcal{V}_2 + \frac{1}{2}\Gamma^{-1}\Theta^2$ whose derivative is

$$\dot{\mathcal{V}}_e = \dot{\mathcal{V}}_1 + \rho\dot{\mathcal{V}}_2 + \Gamma^{-1}\Theta\dot{\Theta}$$

where ρ is the positive weight term for course error in order to make the distance error and course error in the same altitude. Γ is the positive gain for the estimator.

Substitute (5) into the derivative of Lyapunov function $\mathcal{V}_e$

$$\begin{aligned}\dot{\mathcal{V}}_e = \dot{\mathcal{V}}_1 &+ \rho\tilde{\chi}'[i\chi^\infty\frac{2}{\pi}\frac{k}{1+(ke)^2}(\hat{V_g}' - V_g')(\sin\chi' - a\cos\chi') \\ &- \kappa sat(\frac{\tilde{\chi}'}{\epsilon})] + \Gamma^{-1}(\hat{V_g}' - V_g')(\dot{\hat{V}}_g' - \dot{V_g}')\end{aligned}$$

Since V_g' is slowly changing over time, we first assume the derivative of V_g' is negligible. Then the derivative of the Lyapunov function is

$$\begin{aligned}\dot{\mathcal{V}}_e &\approx \dot{\mathcal{V}}_1 + \rho\tilde{\chi}'[i\chi^\infty\frac{2}{\pi}\frac{k}{1+(ke)^2}(\hat{V_g}' - V_g')(\sin\chi' - a\cos\chi') \\ &\quad - \kappa sat(\frac{\tilde{\chi}'}{\epsilon})] + \Gamma^{-1}(\hat{V_g}' - V_g')\dot{\hat{V}}_g' \\ &= \dot{\mathcal{V}}_1 - \rho\kappa\tilde{\chi}' sat(\frac{\tilde{\chi}'}{\epsilon}) + \{\dot{\hat{V}}_g'\Gamma^{-1} + \rho\tilde{\chi}' i\chi^\infty\frac{2}{\pi}\frac{k}{1+(ke)^2} \\ &\quad (\sin\chi' - a\cos\chi')\}(\hat{V_g}' - V_g')\end{aligned}$$

As we have proved before, $\dot{V}_1$ and $-\rho\kappa\tilde{\chi}' sat(\frac{\tilde{\chi}'}{\epsilon})$ are negative semi-definite. So if the derivative of the estimated ground velocity is chosen as:

$$\dot{\hat{V}}_g' = -\Gamma\rho\tilde{\chi}' i\chi^\infty\frac{2}{\pi}\frac{k}{1+(ke)^2}(\sin\chi' - a\cos\chi') \tag{7}$$

The derivative of V_e will be negative semi-definite.

Next, we use Barbalat's Lemma [13] to prove e and $\tilde{\chi}'$ will converge to zero asymptotically.

$$\begin{aligned}\ddot{\mathcal{V}}_e &= \ddot{\mathcal{V}}_1 - \rho\kappa sat(\frac{\tilde{\chi}'}{\epsilon})\dot{\tilde{\chi}}' \\ &= \ddot{\mathcal{V}}_1 - \rho\kappa sat(\frac{\tilde{\chi}'}{\epsilon})[i\chi^{\infty}\frac{2}{\pi}\frac{k}{1+(ke)^2}(\sin\chi' - a\cos\chi')\Theta \\ &\quad - \kappa sat(\frac{\tilde{\chi}'}{\epsilon})]\end{aligned} \tag{8}$$

$\tilde{\chi}$, e and Θ are bounded since $\dot{\mathcal{V}}_e \leq 0$. It also implies $\ddot{\mathcal{V}}_e$ is bounded based on (8). Hence equivalently $\dot{\mathcal{V}}_e$ is uniformly continuous. Combined with the $\mathcal{V}_e$ is bounded and $\dot{\mathcal{V}}_e$ is negative semi-definite. It infers that $\dot{\mathcal{V}}_e$ converges to zero asymptotically according to Barbalat's Lemma, which also means e and $\tilde{\chi}$ converge to zero asymptotically.

Next, we prove that the system is uniformly ultimately bounded under slowly time-varying wind, provided that a σ-modification technique [14] is applied to the adaptive law (7), which results in the adaptive law (6).

Substitute (6) into the derivative of Lyapunov function $\mathcal{V} = \rho\mathcal{V}_2 + \frac{1}{2}\Gamma^{-1}\Theta^2$

$$\begin{aligned}\dot{\mathcal{V}} &= -\rho\kappa\tilde{\chi}' sat(\frac{\tilde{\chi}'}{\epsilon}) + \{(\dot{\hat{V}}_g' - \dot{V}_g')\Gamma^{-1} + \rho\tilde{\chi}' i\chi^{\infty}\frac{2}{\pi}\frac{k}{1+(ke)^2} \\ &\quad (\sin\chi' - a\cos\chi')\}(\hat{V}_g' - V_g') \\ &= -\rho\kappa\tilde{\chi}' sat(\frac{\tilde{\chi}'}{\epsilon}) - \sigma\Theta^2 - \sigma\Theta(-\Gamma^{-1}\dot{V}_g'\sigma^{-1} - V_g')\end{aligned} \tag{9}$$

Using the inequality $-a^2 + ab \leq -\frac{a^2}{2} + \frac{b^2}{2}$ for any a and b, we write

$$\dot{\mathcal{V}} \leq -\rho\kappa\tilde{\chi}' sat(\frac{\tilde{\chi}'}{\epsilon}) - \frac{\sigma}{2}\Theta^2 + \frac{\sigma(V_g' + \dot{V}_g'\Gamma^{-1}\sigma^{-1})^2}{2} \tag{10}$$

Since we assume that the wind changes in a slowly time-varying fashion, the magnitude of $\dot{V}_g'$ will be bounded. And it is evident that the true ground velocity V_g' is bounded. Then the last term in (10) can be modified as

$$\dot{\mathcal{V}} \leq -\rho\kappa\tilde{\chi}' sat(\frac{\tilde{\chi}'}{\epsilon}) - \frac{\sigma}{2}\Theta^2 + C$$

If $\Theta^2 \geq \frac{2C}{\sigma}$, $\dot{\mathcal{V}}$ will be negative definite, which means e,$\tilde{\chi}'$ and Θ will converge inside a ball around the origin and stay bounded. ■

In practice, the estimation of ground velocity rate in (6) (or (7)) is modified with a feedforward term which gives the information on how V_g' changes depending on the course.

$$\begin{aligned}\dot{\hat{V}}_g' &= \frac{\partial V_g'}{\partial\chi'}[i\chi^{\infty}\frac{2}{\pi}\frac{k}{1+(ke)^2}(\sin\chi' - a\cos\chi')\hat{V}_g' - \kappa sat(\frac{\tilde{\chi}'}{\epsilon})] \\ &\quad - \Gamma\rho\tilde{\chi}' i\chi^{\infty}\frac{2}{\pi}\frac{k}{1+(ke)^2}(\sin\chi' - a\cos\chi') - \sigma\Gamma\hat{V}_g'\end{aligned} \tag{11}$$

where the first term in (11) represents $\dot{V}_g'$. The relationship between ground velocity and course can be derived from (1), (2) and (3) [15].

$$V_g' = W'\cos(\psi_w' - \chi') + \sqrt{V_a^2 - W'^2\sin^2(\psi_w' - \chi')} \tag{12}$$

Since the whole wind field is unknown, W' and ψ_w' are substituted with the constant component of wind W and ψ_w in (12). The partial derivative of ground velocity over course is approximately calculated as

$$\begin{aligned}\frac{\partial V_g'}{\partial\chi'} &\approx \frac{\partial V_g}{\partial\chi'} \\ &= W\sin(\psi_w - \chi') + [V_a^2 - W^2\sin^2(\psi_w - \chi')]^{-\frac{1}{2}}W^2 \\ &\quad \sin(\psi_w - \chi')\cos(\psi_w - \chi')\end{aligned} \tag{13}$$

The whole path following strategy for straight line is illustrated in the control scheme in Fig. 2. The control law block includes the modified command course (5). And the estimator block consists of the adaptive law of the estimated ground velocity in (7) or (6) and partial derivative in (13).

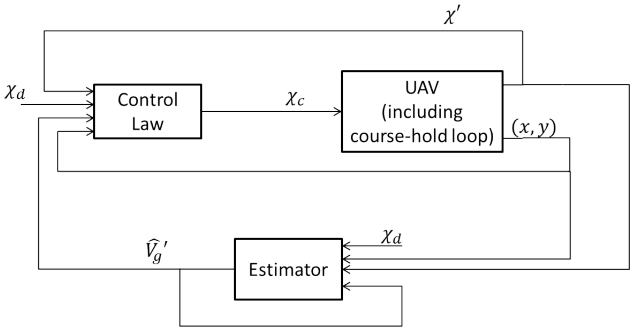

Fig. 2. Scheme of straight line path following

The control scheme is implemented in Simulink, using a desired line described by the equation $y = 0.5x$ in Fig. 3. In order to investigate the influence of control parameters k, κ and ϵ on the performance of straight line following, four different cases of design parameters are compared with each other in Fig. 4. In all simulations, $\sigma = 0$ because this choice delivered good performance and thus it was not necessary to tune this extra parameter.

The design parameters affect the transient behavior of UAV in the following manner. Larger k makes the UAV's transient performance faster. Smaller κ makes the transient trajectory smoother and slower. The parameter ϵ can be tuned to avoid chattering.

The steady state performance of straight line following strategy can be evaluated via the root mean square (RMS) tracking error between the desired path and the real UAV position, excluding the transient tracking errors from the turns. The root mean square error of the four cases in Fig. 4 are summarized in Tab. I. Steady state is assumed when the distance from the desired path settles inside the bounds $\pm 0.1m$.

The performance of the estimator is evaluated with two criteria including transient RMS estimation error and steady

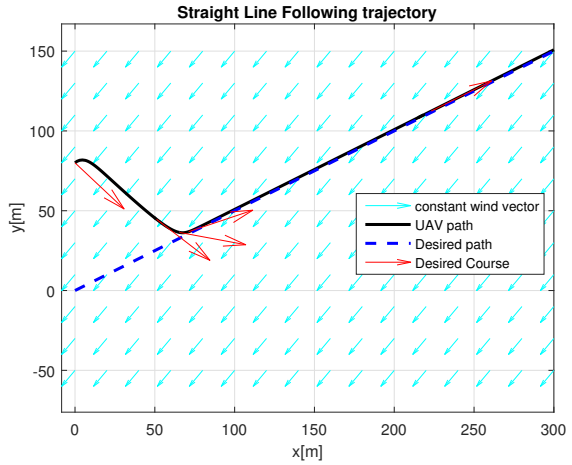

Fig. 3. Straight line following performance

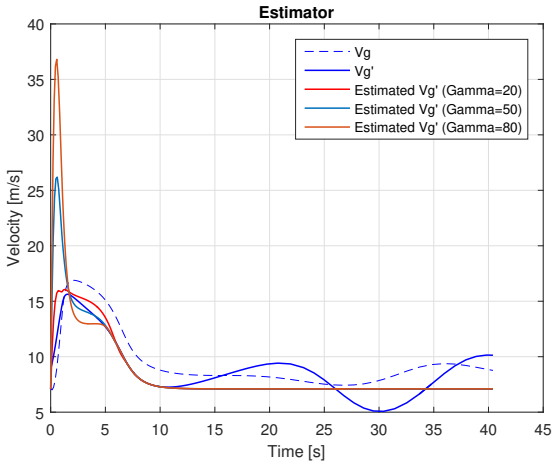

Fig. 5. Estimation performance in straight line following

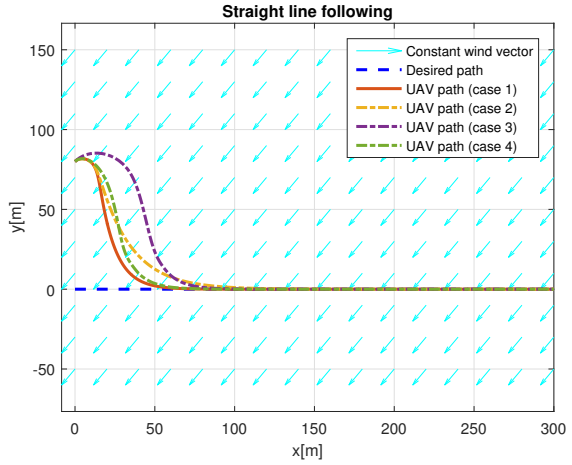

Fig. 4. Influence of design parameters for straight line following:
Case 1: $k = 0.1, \kappa = \frac{\pi}{2}, \epsilon = 0.5, \Gamma = 50$;
Case 2: $k = 0.05, \kappa = \frac{\pi}{2}, \epsilon = 0.5, \Gamma = 50$;
Case 3: $k = 0.1, \kappa = \frac{\pi}{6}, \epsilon = 0.5, \Gamma = 50$;
Case 4: $k = 0.1, \kappa = \frac{\pi}{2}, \epsilon = 1.5, \Gamma = 50$.

RMS estimation error. In Fig. 5, it can be noted that the estimator does not track the real ground velocity. This could be caused by lack of persistence of excitation. Larger estimation gains result in better steady estimation error, but worse transient behavior. The estimator errors for three different estimator gains are collected in Tab. II.

B. Orbit Path Following

The strategy for orbit path following is similar to the straight line following where the vector field is built up around the desired orbit. The UAV position is expressed in the circular coordinates where the origin locates at the orbit center. The distance from the orbit center to the UAV is denoted with d. And the angular position of UAV is denoted with γ. We assume the orbit center (c_x, c_y) and radius r of the desired orbit are known. The relationship between circular coordinates and Cartesian coordinates is

$$\begin{aligned} x &= c_x + d\cos\gamma \\ y &= c_y + d\sin\gamma \end{aligned} \tag{14}$$

Substitute (14) into (2). The dynamics of UAV will be expressed as

$$\begin{aligned} \dot{d} &= V_g'\cos(\chi' - \gamma) \\ \dot{\gamma} &= \frac{V_g'}{d}\sin(\chi' - \gamma) \end{aligned}$$

The desired course which steers the UAV towards the desired path was proposed in [7]

$$\chi_d = \gamma + j[\frac{\pi}{2} + \tan^{-1}(k\tilde{d})]$$

where j indicates the direction of desired orbit. When $j = 1$, a counterclockwise orbit is applied. When $j = -1$, a clockwise orbit is applied. $\tilde{d}$ is the distance error defined as $d - r$.

Similar to the Lyapunov argument for straight line following, the Lyapunov function $\mathcal{V} = \frac{1}{2}\tilde{d}^2 + \frac{1}{2}\rho\tilde{\chi}'^2$ will be used to derive the command course for the UAV. The derivative

TABLE I

TRACKING ERROR FOR 4 DIFFERENT SETS OF DESIGN PARAMETERS

	Case 1	Case 2	Case 3	Case 4
RMS	0.0196	0.0254	0.0185	0.0228

TABLE II

ESTIMATION ERROR FOR 3 ESTIMATOR GAINS

Estimation gain	Transient RMS error	Steady RMS error
$\Gamma = 20$	0.9283	1.6280
$\Gamma = 50$	2.8929	1.6399
$\Gamma = 80$	4.7111	1.5886

of $\mathcal{V}$ is

$$\begin{aligned}\dot{\mathcal{V}} &= \tilde{d}\dot{\tilde{d}} + \rho\tilde{\chi}'\dot{\tilde{\chi}}' \\ &= -V_g'\tilde{d}\sin(\tan^{-1}(k\tilde{d}))+ \\ &\quad \rho\tilde{\chi}'[\alpha(\chi_c - \chi') - \frac{V_g'}{d}\sin(\chi-\gamma) - j\beta V_g'\cos(\chi'-\gamma)]\end{aligned} \tag{15}$$

It is evident that the first term in (15) is always negative. So if the command course is chosen as

$$\chi_c = \chi' + \frac{V_g'}{\alpha d}\sin(\chi-\gamma) + j\frac{\beta}{\alpha}V_g'\cos(\chi'-\gamma) - \frac{\kappa}{\alpha}sat(\frac{\tilde{\chi}'}{\epsilon})$$

$\dot{V}$ will be negative semi-definite, which means that $\tilde{d}, \tilde{\chi}'$ will converge to zero. Since the V_g' is unknown, the control law needs to be modified in a similar manner as the straight line following case. This results in

$$\chi_c = \chi' + \frac{\hat{V}_g{}'}{\alpha d}\sin(\chi-\gamma) + j\frac{\beta}{\alpha}\hat{V}_g{}'\cos(\chi'-\gamma) - \frac{\kappa}{\alpha}sat(\frac{\tilde{\chi}'}{\epsilon}) \tag{16}$$

Theorem III.2: In orbit path following scenario, the command course (16) and the estimator

$$\dot{\hat{V}}_g' = -\Gamma\rho\tilde{\chi}'(\frac{\sin(\chi'-\gamma)}{d} + j\beta\cos(\chi'-\gamma)) - \sigma\Gamma\hat{V}_g{}' \tag{17}$$

with $\Gamma > 0$ being the estimation gain and $\sigma > 0$ being a switching σ-modification parameter, guarantees the tracking error converges to zero for unknown constant winds and stays bounded for unknown slowly time-varying wind.

Proof: The adaptive law of the estimator for the ground velocity is derived in the similar Lyapunov analysis as the straight line following case. Denoted again with $\Theta = \hat{V}_g{}' - V_g'$ as the estimation error. The derivative of the Lyapunov function $\mathcal{V}_e = \mathcal{V} + \frac{1}{2}\Gamma^{-1}\Theta^2$ is

$$\begin{aligned}\dot{\mathcal{V}}_e &= \dot{\mathcal{V}} + \Gamma^{-1}\Theta\dot{\Theta} \\ &= \rho\tilde{\chi}'(\hat{V}_g{}' - V_g')(\frac{\sin(\chi'-\gamma)}{d} + j\beta\cos(\chi'-\gamma)) \\ &\quad - \rho\tilde{\chi}'\kappa sat(\frac{\tilde{\chi}'}{\epsilon}) + \Gamma^{-1}(\hat{V}_g{}' - V_g')(\dot{\hat{V}}_g' - \dot{V}_g{}') \\ &\quad - V_g'\tilde{d}\sin(\tan^{-1}(k\tilde{d}))\end{aligned} \tag{18}$$

First, We assume the changing of ground velocity over course is small enough to be neglected. We obtain

$$\begin{aligned}\dot{\mathcal{V}}_e &\approx \dot{\mathcal{V}} + \Gamma^{-1}\Theta\dot{\Theta} \\ &= -\rho\tilde{\chi}'\kappa sat(\frac{\tilde{\chi}'}{\epsilon}) - V_g'\tilde{d}\sin(\tan^{-1}(k\tilde{d})) \\ &\quad + (\hat{V}_g{}' - V_g')\{\rho\tilde{\chi}'(\frac{\sin(\chi'-\gamma)}{d} + j\beta\cos(\chi'-\gamma)) + \Gamma^{-1}\dot{\hat{V}}_g'\}\end{aligned}$$

If the derivative of the estimated ground velocity is chosen as

$$\dot{\hat{V}}_g' = -\Gamma\rho\tilde{\chi}'(\frac{\sin(\chi'-\gamma)}{d} + j\beta\cos(\chi'-\gamma)) \tag{19}$$

then the derivative of $\mathcal{V}_e$ will be negative semi-definite, which means $\tilde{d}$, $\tilde{\chi}'$ and Θ are bounded. It is easy to find that $\dot{\mathcal{V}}_e$ is also bounded. In another words, $\dot{\mathcal{V}}_e$ is uniformly continuous. Combined with the information $\mathcal{V}_e$ is bounded, it results in $\dot{\mathcal{V}}_e \to 0$ as $t \to \infty$, which indicates that $\tilde{d}$ and $\tilde{\chi}'$ converge to zero asymptotically.

In a similar manner to the straight line following case, we can prove the system is uniformly ultimately bounded under slowly time-varying wind, provided a σ-modification technique [14] is applied to the adaptive law (19). The adaptive law is modified with a small positive design parameter σ as in (17).

Substituting (17) into the derivative of the Lyapunov function (18), we obtain a similar equation as (9). Using the same mathematical derivation, we also conclude that $\tilde{d}$, $\tilde{\chi}'$ and Θ stay bounded. ■

In practice, a feedforward term representing the variation of the wind can be added to (17) (or (19)). We obtain

$$\begin{aligned}\dot{\hat{V}}_g' &= \frac{\partial V_g'}{\partial\chi'}(\frac{\hat{V}_g'}{d}\sin(\chi'-\gamma) + j\beta\cos(\chi'-\gamma) - \kappa sat(\frac{\tilde{\chi}'}{\epsilon})) \\ &\quad - \Gamma\rho\tilde{\chi}'(\frac{\sin(\chi'-\gamma)}{d} + j\beta\cos(\chi'-\gamma)) - \sigma\Gamma\hat{V}_g{}'\end{aligned} \tag{20}$$

where the first term in (20) represents $\dot{V}_g{}'$ and $\frac{\partial V_g'}{\partial\chi'}$ is approximated as (13). The whole control scheme of orbit path following is similar to the straight line following scenario. Fig. 6 illustrates the influence of the design parameters on the performance of orbit path following, using four different choices of design parameters. In all simulations, $\sigma = 0$ because this choice delivered good performance and thus it was not necessary to tune this extra parameter. The RMS tracking errors at steady state are summarized in Tab. III. Case 1 behaves better than the other cases. It indicates that larger k is beneficial for the steady state performance at the expenses of transient performance.

In Fig. 7, the estimator performance for the orbit path following works better than the straight line following since it can track the real ground velocity closely (possibly due to the fact that the circular path generates some persistence of excitation). Larger estimator gain will improve the steady estimation of ground velocity at the expense of large overshoot in transient performance, as summarized in Tab. IV.

TABLE III
TRACKING ERROR FOR 4 DIFFERENT SETS OF DESIGN PARAMETERS

	Case 1	Case 2	Case 3	Case 4
RMS	0.1423	0.2004	0.1921	0.1921

TABLE IV
ESTIMATION ERROR FOR 3 ESTIMATOR GAINS

Estimation gain	Transient RMS error	Steady RMS error
$\Gamma = 20$	2.5419	1.1052
$\Gamma = 50$	3.0363	0.6949
$\Gamma = 80$	3.5641	0.4908

C. Combined Path Following

More complicated paths can be segmented into straight lines and arcs. The strategy for combination of straight lines

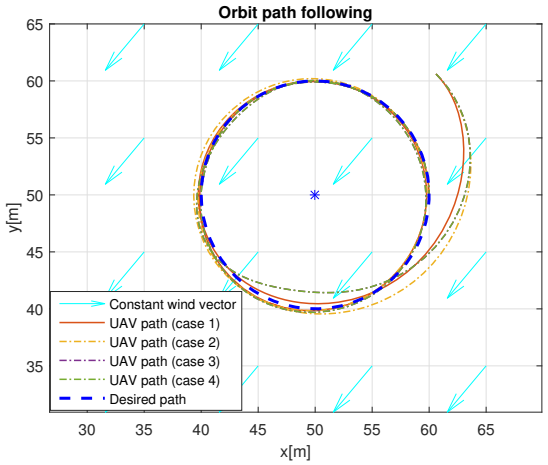

Fig. 6. Influence of design parameters for orbit following:
Case 1: $k = 0.1, \kappa = \frac{\pi}{2}, \epsilon = 0.5, \Gamma = 50$;
Case 2: $k = 0.05, \kappa = \frac{\pi}{2}, \epsilon = 0.5, \Gamma = 50$;
Case 3: $k = 0.1, \kappa = \frac{\pi}{6}, \epsilon = 0.5, \Gamma = 50$;
Case 4: $k = 0.1, \kappa = \frac{\pi}{2}, \epsilon = 1.5, \Gamma = 50$.

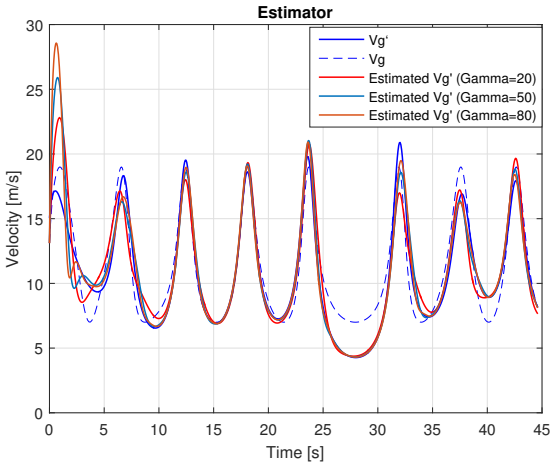

Fig. 7. Estimator performance in orbit path following

and arcs is to build up the vector field around lines and arcs separately and define the transition rules based on distance and angular position. The methods to set up the vector fields for straight lines and arcs are described in the previous parts.

Here is an example to implement the combined path following strategy. The desired path is colored blue in Fig. 8 which looks like an "8" shape. At each of the corners, the vector field transfers from the straight line to the arc if the distance from the UAV to the corner point is within the predetermined range. The vector field transfers from the arc to the straight line if the angular position reaches the predetermined value.

IV. Evaluation of the Algorithm

The comparison among three methods for path following is presented here. The three methods are the standard VF method (which assumes to know the constant wind vector

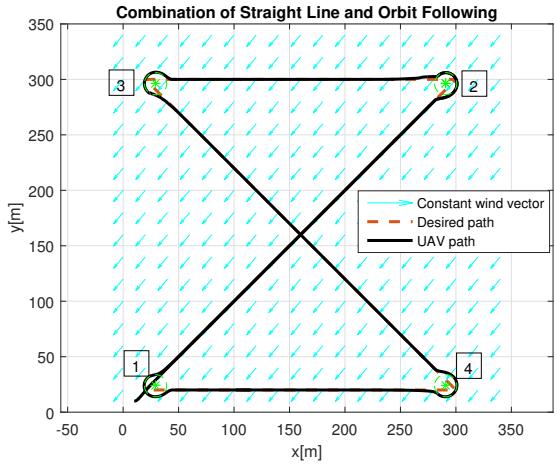

Fig. 8. Combined path following strategy: UAV starts from bottom left and passes waypoints 1, 2, 3, 4 in order.

only), the ideal VF method (which assumes to know both the constant wind vector and the time-varying wind vector) and the proposed adaptive VF method. In details, the standard VF method uses V_g which is the constant part of the ground velocity in the control law; the ideal VF method assumes that the ground velocity V_g' is measurable at any time; the adaptive VF method uses the estimated ground velocity $\hat{V}_g{}'$ in the control law which is more practical compared with the ideal case.

The root mean square error between the desired path and the real path in steady state is used to evaluate the steady state performance of these three methods.

The performance for straight line following is shown in Fig. 9 and Tab. V. For the transient behavior, the proposed method is slightly faster than the others. And the steady state RMS error is smaller than standard VF method. In the same manner, the performance of orbit path following is shown in Fig. 10 and Tab. VI. It is obvious that the proposed adaptive VF method is superior to the standard VF method in both transient and steady state.

TABLE V
Steady state RMS error for straight line following

Method	Standard VF	Ideal VF	Adaptive VF
RMS	0.2203	0.1573	0.1434

TABLE VI
Steady state RMS error for orbit following

Method	Standard VF	Ideal VF	Adaptive VF
RMS	0.33	6.08×10^{-6}	0.1219

V. Conclusion

This paper presented an adaptive vector field method for the UAV path following under slowly time-varying wind environment. The proposed method was developed for two scenarios: straight line following and orbit following. The

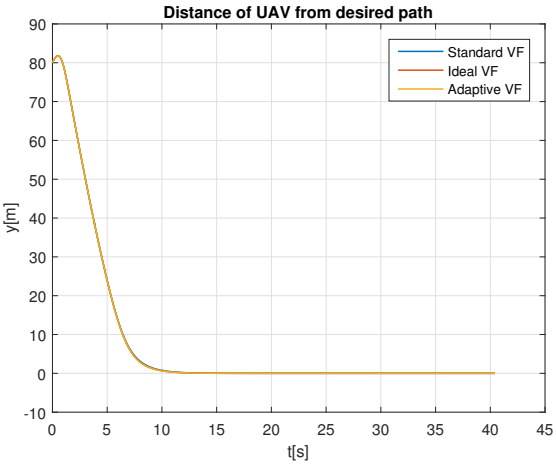

Fig. 9. Distance of UAV from the desired path using 3 different methods

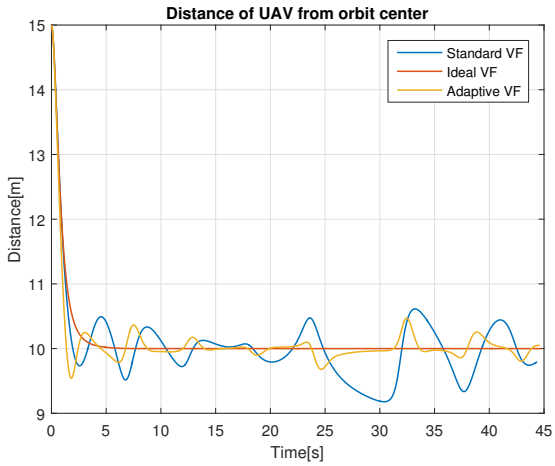

Fig. 10. Distance of UAV from orbit center using 3 different methods

combination of Lyapunov stability argument, σ-modification and Barbalat's Lemma are used to analytically prove that the path following errors are bounded under unknown slowly time-varying winds and converge to zero with unknown constant winds. Numerical simulations have been presented to show the feasibility of the adaptive VF method. The simulations indicate the adaptive VF method has better performance than the standard VF method, especially in the orbit path following scenario. In future works, the adaptive VF method would be implemented on real UAVs and the performance would be tested in practice.

REFERENCES

[1] A. P. Aguiar, J. P. Hespanha, and P. V. Kokotovic, "Performance limitations in reference tracking and path following for nonlinear systems," *Automatica*, vol. 44, no. 3, pp. 598 – 610, 2008.

[2] P. B. Sujit, S. Saripalli, and J. B. Sousa, "Unmanned aerial vehicle path following: A survey and analysis of algorithms for fixed-wing unmanned aerial vehicless," *IEEE Control Systems*, vol. 34, no. 1, pp. 42–59, Feb 2014.

[3] M. Kothari, D. W. Gu, and I. Postlethwaite, "An intelligent suboptimal path planning algorithm using rapidly-exploring random trees," in *Control Conference (ECC), 2009 European*, Aug 2009, pp. 677–682.

[4] A. Ratnoo, P. Sujit, and M. Kothari, "Adaptive optimal path following for high wind flights," *18th IFAC World Congress, Milano*, vol. 44, no. 1, pp. 12 985 – 12 990, 2011.

[5] F. Gavilan, R. Vazquez, and S. Esteban, "Trajectory tracking for fixed-wing uav using model predictive control and adaptive backstepping," *1st IFAC Workshop on Advanced Control and Navigation for Autonomous Aerospace Vehicles ACNAAV15 Seville, Spain*, vol. 48, no. 9, pp. 132 – 137, 2015.

[6] G. Ambrosino, M. Ariola, U. Ciniglio, F. Corraro, E. D. Lellis, and A. Pironti, "Path generation and tracking in 3-d for uavs," *IEEE Transactions on Control Systems Technology*, vol. 17, no. 4, pp. 980–988, July 2009.

[7] D. R. Nelson, D. B. Barber, T. W. McLain, and R. W. Beard, "Vector field path following for miniature air vehicles," *IEEE Transactions on Robotics*, vol. 23, no. 3, pp. 519–529, June 2007.

[8] E. W. Frew, D. A. Lawrence, C. Dixon, J. Elston, and W. J. Pisano, "Lyapunov guidance vector fields for unmanned aircraft applications," in *2007 American Control Conference*, July 2007, pp. 371–376.

[9] H. Chen, K. Chang, and C. S. Agate, "Uav path planning with tangent-plus-lyapunov vector field guidance and obstacle avoidance," *IEEE Transactions on Aerospace and Electronic Systems*, vol. 49, no. 2, pp. 840–856, APRIL 2013.

[10] Y. Liang and Y. Jia, "Combined vector field approach for 2d and 3d arbitrary twice differentiable curved path following with constrained uavs," *Journal of Intelligent & Robotic Systems*, vol. 83, no. 1, pp. 133–160, 2016.

[11] T. A. Johansen, A. Cristofaro, K. Sorensen, J. M. Hansen, and T. I. Fossen, "On estimation of wind velocity, angle-of-attack and sideslip angle of small uavs using standard sensors," *2015 International Conference on Unmanned Aircraft Systems, ICUAS 2015*, pp. 510–519, 2015.

[12] J. D. Barton, "Fundamentals of small unmanned aircraft flight," *Johns Hopkins Apl Technical Digest*, vol. 31, pp. 132–149, 2012.

[13] H. Khalil, *Nonlinear Systems*, ser. Pearson Education. Prentice Hall, 2002.

[14] P. Ioannou, *Adaptive Control Tutorial (Advances in Design and Control)*. Philadelphia, PA, USA: Society for Industrial and Applied Mathematics, 2006.

[15] R. W. Beard and T. W. McLain, *Small unmanned aircraft: Theory and practice*. Princeton University Press, 2012.